Local structures of amorphous and crystalline phases of silica, SiO_2, by neutron total scattering

1999 J. Phys.: Condens. Matter 11 9263

(http://iopscience.iop.org/0953-8984/11/47/311)

J. Phys.: Condens. Matter **11** (1999) 9263–9273. Printed in the UK PII: S0953-8984(99)06785-5

Local structures of amorphous and crystalline phases of silica, SiO_2, by neutron total scattering

David A Keen† and Martin T Dove‡

† ISIS Facility, Rutherford Appleton Laboratory, Chilton, Didcot, Oxfordshire OX11 0QX, UK
‡ Department of Earth Sciences, Cambridge University, Downing Street, Cambridge CB2 3EQ, UK

Received 6 August 1999

Abstract. We quantify the relationship between the atomic structures of the amorphous and the ordered and disordered crystalline phases of silica using neutron total scattering measurements to determine the local atomic configurations. The instantaneous local atomic arrangements of HP-tridymite and β-cristobalite, both dynamically-disordered high-temperature crystalline phases, bear a striking resemblance to the quenched structure of amorphous silica, unlike those of the two phases of quartz and ordered α-cristobalite. The high-temperature phases are not domain averages of their respective low-temperature phases. Our approach has wider application for characterization of disordered crystalline structures in general.

(Some figures in this article appear in colour in the electronic version; see `www.iop.org`)

1. Introduction

Silica has been widely studied because of its importance to both materials science and geology, and also because it has relatively simple crystal structures but a rich phase behaviour [1]. The equilibrium sequence of phase transitions, prior to melting at 1727 °C, is firstly α-quartz to β-quartz (via an incommensurate phase at 574.3 °C), then to HP-tridymite (867 °C), and finally to β-cristobalite (1470 °C). The kinetics of these phase transitions can be extremely sluggish, and there are several other metastable crystalline phases of lower symmetry derived from cooling HP-tridymite and β-cristobalite [1], e.g. α-cristobalite from β-cristobalite below about 280 °C.

All these phases have structures that are infinite frameworks of corner-sharing SiO_4 tetrahedra, with the glass forming a continuous random network [2–4]. The crystalline high-temperature phases HP-tridymite and β-cristobalite consist of identical sheets of corner-sharing SiO_4 tetrahedra (figure 1) joined in an hcp or fcc arrangement respectively. Their ideal, or average, structures have linear Si–O–Si bonds, as illustrated in the top panel of figure 1, which are usually thought to be chemically unreasonable owing to the relatively large energy required to straighten the bond from the more normal bond angles of 145–150°. Instead, it is possible that local disorder of the orientations of the SiO_4 tetrahedra could allow the Si–O–Si bond angles to be lowered to values that are chemically more reasonable, as illustrated in figure 2. On a short length scale these two phases have similar dynamic disorder of the positions of the oxygen atoms. This paper gives a quantitative analysis of this point.

The similarities in bonding, density and position of the first diffraction peak in amorphous silica and β-cristobalite, have led to the suggestion that there is a close structural relationship over short length scales between these two phases [5, 6]. In addition, the observation of

0953-8984/99/479263+11$30.00

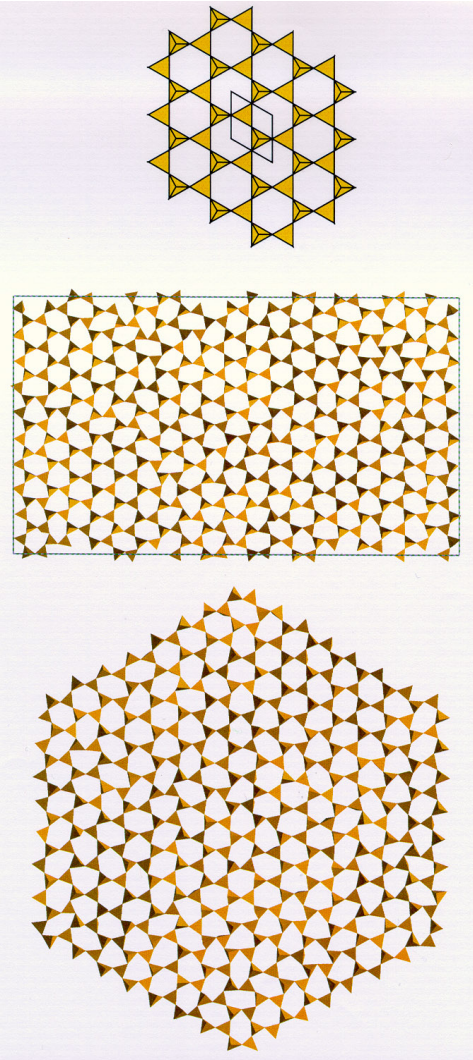

Figure 1. Layers containing hexagonal rings of SiO_4 tetrahedra corresponding to the (001) and (111) layers in HP-tridymite and β-cristobalite respectively. The top panel shows the tetrahedra in ideal orientations, with the hexagonal unit cell of HP-tridymite marked. The middle panel shows a layer of tetrahedra extracted from the RMC refined configuration of HP-tridymite at 550 °C. The bottom panel shows a layer of tetrahedra extracted from the RMC refined configuration of β-cristobalite at 300 °C.

high-pressure amorphization [7] has made the inter-relationship of the silica structures the subject of recent theoretical [8] and molecular dynamics simulation work [9]. In this paper we give the first detailed quantitative analysis of the relationship between the structures of the amorphous and crystalline silica phases over the length scale 0–10 Å obtained from neutron total scattering measurements undertaken on polycrystalline samples of α- and β-quartz, α- and β-cristobalite and HP-tridymite. These measurements give information about both long-range crystallographic order and short-range atomic arrangements. In the high-temperature crystalline phases the structure over short length scales may differ significantly from that corresponding to the "average" structure given by the long-range order. Total scattering measurements are able to provide direct information about this difference.

Accurate and reliable bond lengths and bond angles, independent of the refinement artifacts, are assuming an increased importance in theoretical studies of silica phases [10]. It is often noted that apparent bond lengths from crystal structure refinement have anomalous behaviour on heating. Having described the problems in using crystallographic bond lengths

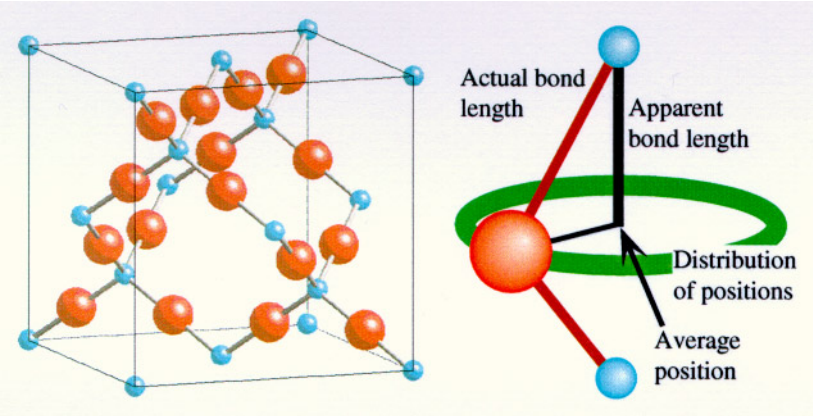

Figure 2. Ideal face-centred cubic crystal structure of β-cristobalite (left) showing linear Si–O–Si bonds and apparent shortening of the Si–O distances. In practice the oxygen atoms have a distribution of positions around the midpoints of the Si–Si vectors, as illustrated on the right, leading to Si–O–Si bond angles nearer 145°.

above (see figure 2) we show here how the actual distribution of bond lengths and bond angles in the disordered silica phases is markedly different from that given by the crystal structure refinements.

2. Method

2.1. Experiment

The neutron total scattering measurements were obtained using the LAD time-of-flight diffractometer at ISIS, with data collected from banks of detectors centred on seven different scattering angles. Powdered samples were contained within a thin-walled cylindrical vanadium can of 8 mm diameter inside a standard neutron furnace with a vanadium foil heater.

The quartz sample was ground from natural crystals. The cristobalite sample was produced by heating silica glass within the cristobalite stability field. The tridymite sample was prepared by a chemical route, and was kindly provided by Professor C M B Henderson (Manchester).

The data reduction involved subtracting measurements of the background signal and making corrections for the attenuation of the neutron beam by the sample, vanadium can, and furnace. A standard silicon sample was used to calibrate the values of $\ell \sin\theta$ for each detector, where ℓ is the total neutron flight path and θ is half the scattering angle. A standard vandium sample was used to calibrate detector efficiencies and to normalize the data onto an absolute scale [11], giving the final total structure factor $F(Q)$.

In addition to forming $F(Q)$, we also used standard normalization procedures to obtain the powder diffraction pattern from the high-angle detectors as a function of flight time (proportional to d-spacing) in order to perform Rietveld refinement of each crystal structure.

2.2. Data analysis

2.2.1. Rietveld analysis. Rietveld analysis was performed on each of the diffraction patterns, using the program TF12LS based on the Cambridge Crystallographic Subroutine Library [12]. This allows refinement of an undulating background (including that due to the diffuse

scattering) by the use of Chebychev polynomials. Full anisotropic temperature factors for all atoms were used in the refinements in order to approximately represent disorder – this led to a significant improvement in the agreement of the calculated diffraction pattern with the data, and did not lead to a significant non-spherical distribution of the positions of the silicon atoms. The refined anisotropic thermal parameters for the oxygen atoms are large and elongated in the plane that bisects the Si–Si vector as expected from the distribution of oxygen positions indicated in figure 2—this has been described in detail for β-cristobalite [13]. The refinements were based on published structures of each phase [1].

2.2.2. Total scattering measurements. In total scattering measurements, the corrected total structure factor $F(Q)$ contains the Bragg and diffuse scattering, and can be cast in terms of the total radial distribution functions $G(r)$ or $T(r)$:

$$F(Q) = \rho \int_0^\infty 4\pi r^2 G(r) \frac{\sin(Qr)}{Qr} \mathrm{d}r \tag{1}$$

$$G(r) = \sum_{i=1}^{n} \sum_{j=1}^{n} c_i c_j b_i b_j \left[g_{ij}(r) - 1 \right] \tag{2}$$

$$T(r) = r\left[G(r) \Big/ \sum_i (c_i b_i)^2 + 1 \right] \tag{3}$$

c_i and b_i are the proportion and neutron scattering length respectively of atom type i, and $g_{ij}(r)$ are the partial radial distribution functions which correlate the distances between atoms i and j at an instant of time. In a crystalline material, the Bragg peaks, which are purely elastic scattering, give the time-average periodic structure. On the other hand, $F(Q)$, which contains the total scattered intensity integrated over all energies, gives information about the instantaneous structure through pair correlation functions, and thereby information about fluctuations in the structure away from the average structure.

When a crystal structure is dynamically disordered, the time-averaged periodic and instantaneous local structures may be very different. The time-average structure, obtained from the Rietveld refinement, gives the separations between the average atomic positions. On the other hand, the peak positions in $T(r)$ give a direct measure of the instantaneous interatomic separations, which invariably will be slightly longer than the separations between the average positions. The overall $T(r)$ functions from the different samples are shown in figure 3, together with the partial radial distribution functions $g_{ij}(r)$ using the methods described below.

2.2.3. Reverse Monte Carlo refinement. In order to investigate the disordered structures further, we have produced three-dimensional structures that are fully consistent with the average and instantaneous structures using the reverse Monte Carlo (RMC) technique [14], adapted to refine a constrained initial structure [15, 16]. The initial structure is maintained by requiring the SiO_4 tetrahedra to remain of regular size and shape, with the length of the Si–O bond determined from the lowest-r peak in $T(r)$, and by retaining the connectivity between atoms in the structure. The tetrahedra are then allowed to relax with Gaussian distributions of widths $\sigma_{\mathrm{Si-O}}$ and $\sigma_{\mathrm{O-Si-O}}$ about the mean Si–O bond length ($R_{\mathrm{Si-O}}$) and the ideal tetrahedral O–Si–O bond angle ($\Theta_{\mathrm{O-Si-O}}$), so that they approximately reproduce the low-r peak widths in $T(r)$. The model is then refined by requiring the calculated $F(Q)$ to fit the experimental $F(Q)$, by slowly increasing the weighting of the fit to $F(Q)$ with respect to the constraints until good

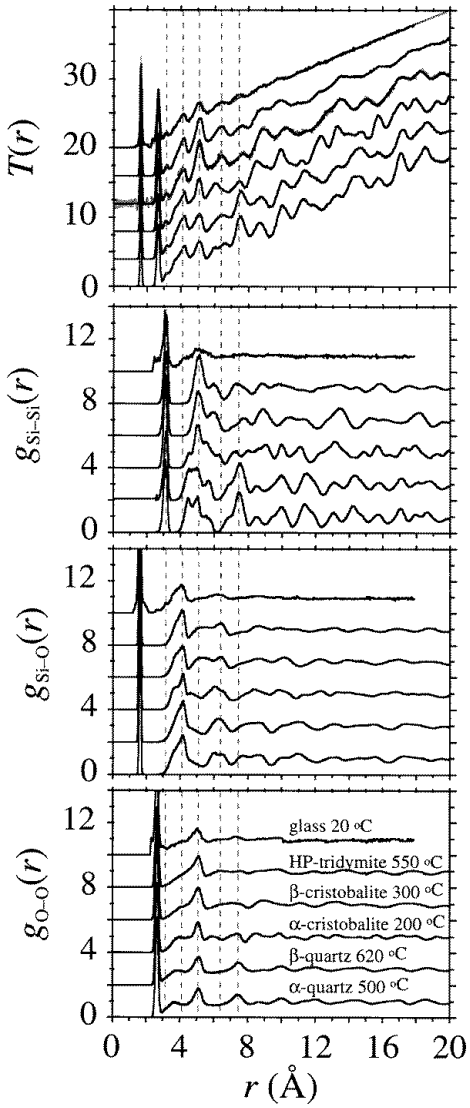

Figure 3. Total and partial radial distribution functions $T(r)$ and $g_{ij}(r)$ obtained from the RMC analysis (successive functions are offset vertically by 2 for clarity, and the labelling in the bottom plot is the same for all plots). Dashed lines correspond to the positions of the distinct peaks in the glass $T(r)$ above 3 Å. The two peaks below 3 Å are the Si–O and O–O distances within the SiO_4 tetrahedra. The direct transformed $T(r)$ for β-cristobalite and the calculated $T(r)$ for amorphous silica (see text for details) are both shown superimposed on their respective RMC generated $T(r)$.

agreement is obtained. Formally, the agreement is defined by

$$\chi^2 = \sum_{i=1}^{N} \left[F_{\mathrm{calc}}(Q_i) - F_{\mathrm{exp}}(Q_i)\right]^2 / \sigma^2(Q_i) + \sum_{\text{Si–O bonds}} \left[r_{\mathrm{Si-O}} - R_{\mathrm{Si-O}}\right]^2 / \sigma^2_{\mathrm{Si-O}} + \sum_{\text{O–Si–O angles}} \left[\theta_{\mathrm{O-Si-O}} - \Theta_{\mathrm{O-Si-O}}\right]^2 / \sigma^2_{\mathrm{O-Si-O}} \quad (4)$$

where N is the number of different values of Q in the data, 'calc' and 'exp' refer to the calculated and experimental quantities respectively, $r_{\mathrm{Si-O}}$ is a Si–O bond length, and $\theta_{\mathrm{O-Si-O}}$ is an O–Si–O angle. In principle the weighting parameters $\sigma(Q_i)$ are determined by the experimental error on each data point, but in practice they were treated as a single parameter (independent

of Q) that was adjusted to change the relative importance of the data and constraints in the refinement.

In each crystalline case, the starting model was produced from atom coordinates obtained from Rietveld refinement of our data. The starting glass model and refinement details are described in [15, 16]. Configurations of around 20 000 atoms (varying from phase to phase) were used with periodic boundary conditions, and an identical fitting procedure was used in each case. The agreement between the experimental $F(Q)$ and the direct transformed $T(r)$ from the RMC was excellent in each case. Spatial averaging showed that the atom density distributions were consistent with the Rietveld refined temperature factors.

3. Results

3.1. Bond lengths

The separations of the *average* positions of the atoms within the SiO_4 tetrahedra obtained from the Rietveld analysis are given in table 1, and compared with the average instantaneous interatomic distances obtained from the peaks in the $g_{ij}(r)$ and $T(r)$ functions (figure 3). The average structures of the disordered crystalline silica phases obtained from Rietveld refinement of the Bragg peaks show an apparent contraction of the SiO_4 tetrahedra. We note that although the bond lengths from Rietveld analysis may be quoted to high precision, they are based on average atom positions which in the simplest systems (such as β-cristobalite) may be derived solely from the lattice parameters. In contrast, the less precise bond lengths obtained from $T(r)$ do incorporate the effect of thermal disorder and are more representative of the local structure. These do not show a contraction of the SiO_4 tetrahedra.

Table 1. Bond lengths, angles and atomic densities (ρ) for the ambient-pressure phases of silica at various temperatures. The data not in brackets are from analysis of the crystal structures from the Rietveld analysis, the data in round brackets are obtained from the $T(r)$ data, and the data in square brackets are obtained from analysis of the RMC configurations (with FWHM of the distributions given in brackets). Data for the glass are from [15, 16]. Typical errors on bond lengths from Rietveld analysis are in the fourth decimal place, whereas those from fitting the peaks in $T(r)$ are one or two in the last decimal place quoted.

	α-quartz	α-quartz	β-quartz	α-cristobalite	β-cristobalite	HP-tridymite	Glass
T (°C)	20	500	620	200	300	550	20
ρ (Å^{-3})	0.0795	0.0773	0.0761	0.0692	0.0661	0.0655	0.0657
Si–Si (Å)	3.059	3.081	3.093	3.077	3.089	3.068/3.109	—
	(3.06)	(3.11)	(3.12)	(3.08)	(3.11)	(3.10)	(3.10)
Si–O (Å)	1.609	1.602	1.588	1.597	1.544	1.534,1.555	—
	(1.609)	(1.612)	(1.613)	(1.606)	(1.606)	(1.613)	(1.617)
O–O (Å)	2.616–2.645	2.601–2.628	2.565–2.611	2.590–2.636	2.522	2.532	—
	(2.632)	(2.626)	(2.627)	(2.623)	(2.623)	(2.634)	(2.626)
O–Si–O (°)	108.7–110.5	108.4–110.3	107.8–110.6	108.3–111.2	109.5	108.8/110.1	—
	(109.8)	(109.1)	(109.0)	(109.5)	(109.5)	(109.5)	(108.6)
	—	[109(5)]	[109(5)]	[109(5)]	[109(5)]	[109(5)]	[109(7)]
Si–O–Si (°)	143.7	148.5	153.9	148.9	180	180	—
	(144)	(149)	(151)	(147)	(151)	(148)	(147)
	—	[145(14)]	[148(15)]	[144(11)]	[148(15)]	[150(16)]	[144(21)]
Si–Si–Si (°)	91.2,106.9,	91.1,107.5,	91.1,107.9,	94.5,108.5,	109.5	109.2,109.7	—
	123.3,141.6	126.3,138.5	132.3	124.2			
	—	[91(5),107(5),	[93(4), 108(6),	[93(4), 108(6),	[109(8)]	[109(8)]	[106(28)]
		125(5),139(7)]	125(5)]	125(5)]			

3.2. Comparisons of the $T(r)$ functions for the crystalline phases

A key result from the comparison of the $g_{ij}(r)$ and $T(r)$ functions for the two crystalline phases of cristobalite in figure 3 is that there are significant differences for distances greater than 5 Å. This dispels a popular theory that β-cristobalite is merely a collection of ordered α-cristobalite domains [17]. In fact the RMC configurations of β-cristobalite, figure 1, do not show domains of any symmetry. Moreover, domains of α-quartz are not found in the RMC configurations of β-quartz. This is reflected in the small differences in the peaks in the radial distribution functions in the range 5–10 Å.

3.3. Comparison of the $T(r)$ functions for the crystalline and amorphous phases

From figure 3 we also find a remarkable correspondence between the radial distribution functions from HP-tridymite, β-cristobalite and the glass. The oscillations in $T(r)$ for HP-tridymite and β-cristobalite remain in phase until well above 10 Å and there is very little to distinguish between HP-tridymite and glass in the $g_{ij}(r)$ apart from the longer-range oscillations in HP-tridymite.

We can make a simple quantitative comparison of the structure of amorphous silica with HP-tridymite and β-cristobalite by assuming that the correlation between the local structures of the amorphous and crystalline phases decays exponentially with a correlation length ξ. Thus we can approximate $g(r)$ for the glass as a sum of a contribution from the (disordered) crystal structure, $g_{\mathrm{crystal}}(r)$, and from a random, $g_{\mathrm{random}}(r)$, arrangement:

$$\begin{aligned} g_{\mathrm{glass}}(r) &= \exp(-r/\xi)g_{\mathrm{crystal}}(r) + \left[1 - \exp(-r/\xi)\right] g_{\mathrm{random}}(r) \\ &= \exp(-r/\xi)\left[g_{\mathrm{crystal}}(r) - 1\right] + 1 \end{aligned} \tag{5}$$

where $g_{\mathrm{random}}(r) = 1$. We have constructed $g_{\mathrm{glass}}(r)$ using the RMC results for HP-tridymite (rather than β-cristobalite since the orientational order in HP-tridymite more closely resembles that in the glass, as discussed below). The best fit for the partial $g(r)$ functions is obtained using a correlation length of $\xi = 7.5$ Å for $g_{\mathrm{Si-O}}(r)$ and $\xi = 11$ Å for $g_{\mathrm{O-O}}(r)$. Figure 3 includes, for comparison with the actual data, the overall $T(r)$ for the glass reconstructed from the individual $g_{\mathrm{glass}}(r)$ that were calculated using the HP-tridymite data and a value of $\xi = 7.5$ Å in Equation (5). It can be seen that this resembles the measured $T(r)$ for silica glass reasonably well. Thus we can say that the similarities between the crystalline and amorphous phases extends over the length scale of ξ. For comparison, the average length (Si to Si) across a ring of six SiO_4 tetrahedra in the disordered crystalline phases is about 6 Å. ξ is therefore too short to admit a "microcrystalline" interpretation of the glass structure, and one cannot say that the structures are *identical* over this length scale. Instead, this result indicates that up to the distance ξ there are regions of the glass that have the structure elements of the crystal, and beyond this distance the differences between crystal and glass diverge.

The finite range of the correlations between the amorphous and crystalline structures are highlighted by the orientational relationships between neighbouring SiO_4 tetrahedra. The distributions of Si–O–Si bond angle θ, $f(\theta)$, deduced from the RMC configurations are shown in figure 4. The similarities between the two disordered crystalline phases and the glass are striking. For the disordered phases, we found that there is no prefered orientation of the Si–O–Si plane with respect to the orientations of the SiO_3 pyramids of the rest of the tetrahedra—the middle atoms in the Si–O–Si bonds lie uniformly distributed on an annulus around the Si–Si vector. As an interesting aside, we have also investigated any correlations between θ and the Si–O bond length, and contrary to quantum chemical calculations [18, 19] we find that there is no correlation in any of the phases. The distributions of the torsional angles ϕ, $g(\phi)$ (figure 4) show rather more contrast between the disordered phases. In β-cristobalite, the

crystallographic symmetry gives a mean value $\phi = 60^\circ$, which is reflected in the calculated form of $g(\phi)$. However, there is a wide distribution in the torsional angles: $g(\phi)$ has a full width of 54°. In HP-tridymite, the crystallographic symmetry gives mean values of $\phi = 60^\circ$ for 75% of the pairs of neighbouring tetrahedra, and $\phi = 0^\circ$ for remaining pairs. Again, there is a wide distribution about each mean value, with a width of about 47°. By contrast, the distribution $g(\phi)$ for silica glass is virtually constant for all ϕ. To appreciate the difference we note that a distribution with two peaks of equal heights and widths of around 50° centred on $\phi = 0^\circ$ and $\phi = 60^\circ$ will give a nearly-flat distribution $g(\phi)$. In this regard, the glass can simply be seen to have a similar $g(\phi)$ to HP-tridymite without the crystallographic constraints on mean values of ϕ.

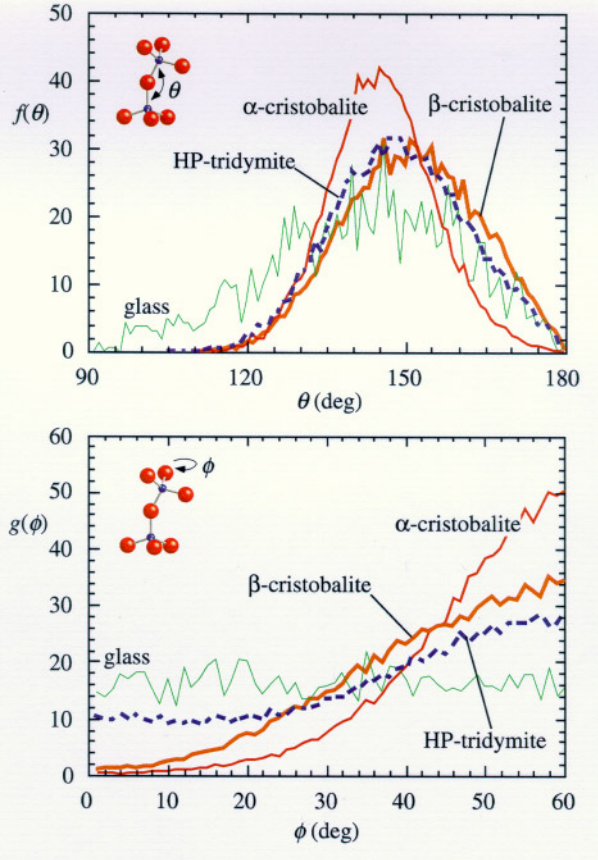

Figure 4. Bond angle distribution functions; the upper plot shows $f(\theta)$ for the Si–O–Si bonds, and the lower plot shows $g(\phi)$ of the torsional angles. The angles are defined in the top corners of each diagram.

3.4. Calculation of three-dimensional diffuse scattering pattern for β-cristobalite

In general, RMC modelling of a single one-dimensional diffraction pattern may not necessarily produce a unique three-dimensional structure. However, by careful use of chemical constraints and an appropriate starting structure, models produced by RMC refinement may be able to reproduce the three-dimensional short-range disordered structure faithfully. To test this, we

have calculated the diffuse scattering from β-cristobalite in the $(hk0)$ section of the three-dimensional reciprocal lattice directly from the RMC configurations, figure 5. This shows a set of well-defined streaks along the $\langle 100 \rangle$ and $\langle 110 \rangle$ directions in reciprocal space. These streaks are fully consistent with the streaks of diffuse scattering observed in electron diffraction studies of β-cristobalite [20, 21], and also with the set of calculated low-energy rigid unit modes [22–24]. From this result we have established that RMC refinement with appropriate constraints (which themselves are based on the data) is able to reproduce the full three-dimensional structure of the disordered crystals accurately.

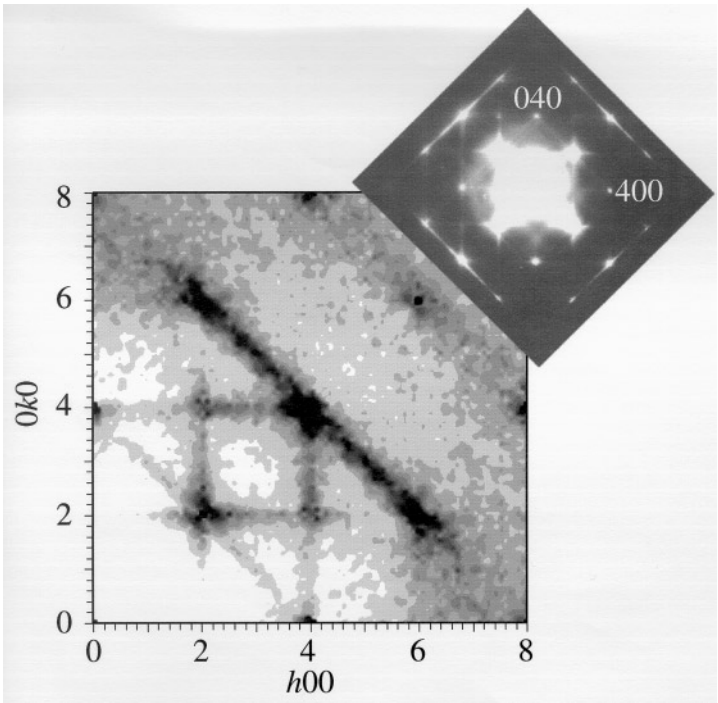

Figure 5. Diffuse scattering from β-cristobalite at 300° calculated from the RMC configurations. The lines of diffuse scattering correspond to the predictions of the RUM model [22–24]. Experimental TEM data [20], which show the same lines are shown as the insert in the top right corner.

4. Discussion: the similarites between the local structures of amorphous and crystalline silica

The structural similarities between β-cristobalite, HP-tridymite and amorphous silica over the length scale 0–10 Å can now be interpreted in terms of the internal flexibility of the cristobalite and tridymite structures as deduced using the rigid unit mode model [23], which is concerned with ways in which the structure can distort by rotations and displacements of undeformed SiO_4 tetrahedra. This model, confirmed by diffuse electron [20, 21] and inelastic neutron [24] scattering measurements, shows that there is far more internal flexibility in the β-cristobalite and HP-tridymite structures than in any of the corresponding low temperature phases or the quartz phases. Since the disordered glass structure needs considerable flexibility of the shapes of the rings of linked tetrahedra in order to form a continuous random network, it is not

surprising that the glass structure uses structural elements of these flexible phases. As a result the local structural elements from the β-cristobalite and HP-tridymite structures in the glass will be distorted and therefore unlike the ideal structures of these phases.

By inverting the above argument, this internal flexibility will distort the local structures of the crystalline phases to give disorder similar to that found in the glass. The ideal structures of β-cristobalite and HP-tridymite, as noted above, have linear Si–O–Si bonds, and the tetrahedra rotate within the allowed rigid unit mode flexibility to change the bond angle to a more favourable value. This is illustrated in figure 1, which shows how the local disorder is accommodated within the layers of the average structures of β-cristobalite and HP-tridymite with displaced and rotated SiO_4 tetrahedra on a regular lattice. The wide distribution of ring shapes (which would be perfect hexagons within the ideal structure) is strongly reminiscent of the glass structure †. In the crystalline phases this disorder is dynamic, arising from the RUM phonons supported by the underlying periodic structure and driven by the need to avoid local configurations with linear Si–O–Si bonds, whereas in the glass the disorder is static, forced by the topological disorder which does not change over short time scales. The low-temperature ordered phases do not have the same flexibility as the high-temperature crystalline phases, and as a result have little similarity with the glass phase.

Although we have only shown results from a single compound, RMC refinement of the structural disorder in a crystalline material using neutron total scattering is a completely general technique. Time-of-flight neutron diffraction provides high quality Bragg data for Rietveld refinement and total scattering data from the same measurement. RMC refinement produces structural models which are internally consistent with the average (Rietveld refined) and instantaneous structures. With the use of appropriate constraints, RMC refinement could be used to characterize the structural disorder in (for example) more complex silicate structures such as zeolites [25], orientationally disordered crystals such as C_{60} [26] or the various phases of ethanol [27, 28], locally distorted structures such as CMR materials [29] or even ionic conductors [30].

In conclusion, we have shown experimentally that the structure of amorphous silica over the length scale 0–10 Å has similarities with that of β-cristobalite and HP-tridymite, but is dissimilar to either phase of quartz or α-cristobalite. The similarities can be understood in terms of the increased flexibility of the two disordered crystalline phases. We have been able to determine the local structures of these disordered crystalline systems by marrying the opportunities of total scattering and Rietveld refinement via computer modelling. This has not only allowed us to make a direct experimental determination of the locally disordered crystal structures but also to compare the corresponding glass and crystal structures directly and quantitatively.

References

[1] Heaney P J 1994 *Rev. Mineral.* **29** 1
[2] Zachariasen W H 1932 *J. Am. Chem. Soc.* **54** 3841
[3] Wright A C 1994 *J. Non-Cryst. Sol.* **179** 84
[4] Grimley D I, Wright A C and Sinclair R N 1990 *J. Non-Cryst. Solids* **119** 49
[5] Le Bail A J 1995 *Non-Cryst. Solids* **183** 39
[6] Gaskell P H and Wallis D J 1996 *Phys. Rev. Lett.* **76** 66
[7] Hemley R J, Jephcoat A P, Mao H K, Ming L C and Manghnani M H 1988 *Nature* **334** 52
[8] Dmitriev V, Torgashev V, Toledano P and Salje E K H 1997 *Europhys. Lett.* **37** 553
[9] Wentzcovitch R M, da Silva C and Chelikowsky J R 1998 *Phys. Rev. Lett.* **80** 2149

† The dynamics of the ring distortions have been studied using molecular dynamics simulations, and can be viewed on the WWW at http://www.esc.cam.ac.uk/rums.

[10] Demuth Th, Jeanvoine Y, Hafner J and Ángyán J G 1999 *J. Phys.: Condens. Matter* **11** 3833
[11] Howe M A, McGreevy R L and Howells W S 1989 *J. Phys.: Condens. Matter* **1** 3433
[12] David W I F, Ibberson R M and Matthewman J C 1992 Rutherford Appleton Laboratory Report RAL-92-031
[13] Schmahl W W, Swainson I P, Dove M T and Graeme-Barber A 1992 *Zeit. für Krist.* **201** 125
[14] Keen D A and McGreevy R L 1990 *Nature* **344** 423
[15] Keen D A 1997 *Phase Transitions* **61** 109
[16] Keen D A 1997 in *Local Structure from Diffraction* ed M F Thorpe and S Billinge (New York: Plenum) pp 101–120
[17] Hatch D M and Ghose S 1991 *Phys. Chem. Min.* **17** 554
[18] Lasaga A C and Gibbs G V 1987 *Phys. Chem. Min.* **14** 107
[19] Lasaga A C and Gibbs G V 1988 *Phys. Chem. Min.* **16** 29
[20] Hua G L, Welberry T R, Withers R L and Thompson J G 1988 *J. Appl. Cryst.* **21** 458
[21] Dove M T, Hammonds K D, Heine V, Withers R L and Kirkpatrick R J 1996 *Phys. Chem. Min.* **23** 55
[22] Hammonds K D, Dove M T, Giddy A P, Heine V and Winkler B 1996 *Am. Min.* **81** 1057
[23] Dove M T, Heine V, Hammonds K D, Ghambhir M and Pryde A K A 1998 in *Local Structure from Diffraction* ed M F Thorpe and S Billinge (New York: Plenum) pp 253–72
Hammonds K D, Dove M T, Giddy A P, Heine V and Winkler B 1996 *Am. Min.* **81** 1057
[24] Swainson I P and Dove M T 1993 *Phys. Rev. Lett.* **71** 193
[25] Hammonds K D, Deng H, Heine V and Dove M T 1997 *Phys. Rev. Lett.* **78** 3701
[26] Glas R, Blaschko O, Krexner G, Haluska M and Kuzmany H 1994 *Phys. Rev.* B **50** 692
[27] Fayos R, Bermejo F J, Dawidowski J, Fischer H E and Gonzalez M A 1996 *Phys. Rev. Lett.* **77** 3823
[28] Bermejo F J, Criado A, Fayos R, Fernandez-Perea R, Fischer H E, Suard E, Guelylah A and Zuniga J 1997 *Phys. Rev.* B **56** 11536
[29] Billinge S J L, Difrancesco R G, Kwei G H, Neumeier J J and Thompson J D 1996 *Phys. Rev. Lett.* **77** 715
[30] Keen D A and Hull S 1998 *J. Phys.: Condens. Matter* **10** 8217